Chemistry–A European Journal
Research Article
doi.org/10.1002/chem.202104161
Chemistry Europe
European Chemical Societies Publishing
www.chemeurj.org

Bright Luminescence by Combining Chiral [2.2]Paracyclophane with a Boron–Nitrogen-Doped Polyaromatic Hydrocarbon Building Block

Mario R. Rapp,[a] Wolfgang Leis,[b] Francesco Zinna,[c] Lorenzo Di Bari,[c] Tamara Arnold,[a] Bernd Speiser,[a] Michael Seitz,[b] and Holger F. Bettinger*[a]

Abstract: Novel BN-doped compounds based on chiral, tetrasubstituted [2.2]paracyclophane and NBN-benzo[*f*,*g*]tetracene were synthesized by Sonogashira–Hagihara coupling. Conjugated ethynyl linkers allow electronic communication between the π-electron systems through-bond, whereas through-space interactions are provided by strong π–π overlap between the pairs of NBN-building blocks. Excellent optical and chiroptical properties in racemic and enantiopure conditions were measured, with molar absorption coefficients up to $\varepsilon = 2.04 \times 10^5\ M^{-1}\,cm^{-1}$, fluorescence quantum yields up to $\Phi_{PL} = 0.70$, and intense, mirror-image electronic circular dichroism and circularly polarized luminescence signals of the magnitude of 10^{-3} for the absorption and luminescence dissymmetry factors. Computed $g_{lum,calcd.}$ values match the experimental ones. Electroanalytical data show both oxidation and reduction of the ethynyl-linked tetra-NBN-substituted paracyclophane, with an overlap of two redox processes for oxidation leading to a diradical dication.

Introduction

Conjugated organic compounds are of ever-growing importance for modern technology.[1–7] They can provide superior characteristics over inorganic alternatives, such as flexibility in the solid state, enhanced charge transfer capabilities, and favorable optical properties,[8–10] while also offering the opportunity for easy modification. In the case of emitting compounds, due to the quantum mechanical property of being a massless boson with spin $\pm 1\,\hbar$, each generated photon can be in one of two circularly polarized states: either left or right handed circularly polarized.[11] For achiral emitting samples both states become equally populated, therefore the net polarization of the emitted light beam is zero. This changes for chiral luminescent systems in enantiopure or enantioenriched samples.[12] The absence of improper rotation symmetry elements allows for the favored emission of photons with one of the two possible polarizations, effectively transmitting molecular chirality to the light beam.[13] The differential emission of left- and right-handed circularly polarized light can be measured through circularly polarized luminescence (CPL) spectroscopy and is quantified by the luminescence dissymmetry factor g_{lum}, calculated as $g_{lum} = 2\Delta I(\lambda)/I(\lambda)$, where $\Delta I(\lambda) = I_L(\lambda) - I_R(\lambda)$ and $I(\lambda) = I_L(\lambda) + I_R(\lambda)$.[14] The value of g_{lum} is therefore ranging from -2 to $+2$. For chiroptical applications, a high value of $|g_{lum}|$ is desirable; however, isolated chiral organic molecules usually exhibit relatively small dissymmetry factors of about 10^{-4}–10^{-2},[12] but offer several other advantages as discussed above. In addition to a high $|g_{lum}|$, for many applications a high photoluminescence (PL) quantum yield and extinction coefficient are necessary.[15] Potential applications for organic chromophores capable of circularly polarized emission are in the fields of &bk(bio-)assay probing, sensing, asymmetric synthesis, and display and optical storage devices.[15–18]

One class of planar chiral organic compounds are mono-substituted or appropriately multisubstituted regioisomers of [*n.n*]paracyclophanes (PCP). Short aliphatic bridges between the phenylene rings hinder free rotation, thus making the compounds conformationally stable.[19] Especially the [2.2]PCP with two short ethylene bridges offers not only a planar chiral scaffold, but also a heavily strained structure with cofacial phenylene rings in close vicinity.[20] Their distance of around 3 Å[21] is substantially shorter than the van der Waals distance found in arene crystals, making them prone to transannular interactions.[19] By extension of the π-system of the [2.2]PCP and introduction of chromophore substituents their absorption and emission properties should be significantly altered and potentially improved for (chir-)optical applications. This approach has been used by Morisaki and Chujo *et al.*, who have been very

[a] M. R. Rapp, T. Arnold, Prof. Dr. B. Speiser, Prof. Dr. H. F. Bettinger
Institut für Organische Chemie, Universität Tübingen
Auf der Morgenstelle 18, 72076 Tübingen (Germany)
E-mail: holger.bettinger@uni-tuebingen.de
[b] Dr. W. Leis, Prof. Dr. M. Seitz
Institut für Anorganische Chemie, Universität Tübingen
Auf der Morgenstelle 18, 72076 Tübingen (Germany)
[c] Dr. F. Zinna, Prof. Dr. L. Di Bari
Department of Chemistry and Industrial Chemistry
Università di Pisa
56124 Pisa (Italy)

Supporting information for this article is available on the WWW under https://doi.org/10.1002/chem.202104161

© 2021 The Authors. Chemistry - A European Journal published by Wiley-VCH GmbH. This is an open access article under the terms of the Creative Commons Attribution Non-Commercial License, which permits use, distribution and reproduction in any medium, provided the original work is properly cited and is not used for commercial purposes.

© 2021 The Authors. Chemistry - A European Journal published by Wiley-VCH GmbH

active in the field of optically active chiral [2.2]paracyclophanes in recent years, successfully designing conjugated microporous polymers, dendrimers and 3D propeller-like structures with exceptionally high $|g_{lum}| = 1.1 \times 10^{-2}$.[22–26] Others have developed PCP-based compounds capable of thermally activated delayed fluorescence or solvent-induced switching of the CPL sign.[27,28]

Formal substitution of polycyclic aromatic hydrocarbons (PAHs) with boron–nitrogen (BN) units that are isoelectronic to a CC pair is a common way in organic materials science to modify the electronic properties of a compound without altering its structure.[29–31] This technique is used for the design of compounds for applications as semiconducting and optoelectronic materials.[32–37] However, there are very few examples of the investigation of BN-doped chiral PAHs towards their CPL activity. One of the exceptions are several NBN-heterohelicenes featuring NBN-heteroacene subunits with high fluorescence quantum yields up to $\Phi_{PL} = 0.83$ associated to CPL signals with $|g_{lum}| = 7.5 \times 10^{-4}$ reported by Sun *et al.*, certifying that such structures can have desirable chiroptical properties.[38] To our knowledge, BN-doped PAHs have not been attached as substituents to [2.2]PCP scaffolds, such as the chiral 4,7,12,15-tetrasubstituted [2.2]PCP, yet. Close proximity of the BN-PAH pendants and bonding to the [2.2]PCP core aromatic system through ethynyl linkers potentially allows for electronic communication of the π-systems through-space and through-bond. Paired with the induced chirality by the conformationally stable [2.2]PCP building block this could prove to be a successful approach towards new chiroptically active materials.

Here we have combined the [2.2]PCP core with four photoluminescent NBN-benzo[*f*,*g*]tetracene (**1**) subunits (Φ_{PL} = 0.24;[39] Scheme 1) and report racemic *rac*-**6**, as well as enantiopure forms (*R*)-**6**, (*S*)-**6**, and the characterization of (chir-)optical and electrochemical properties.

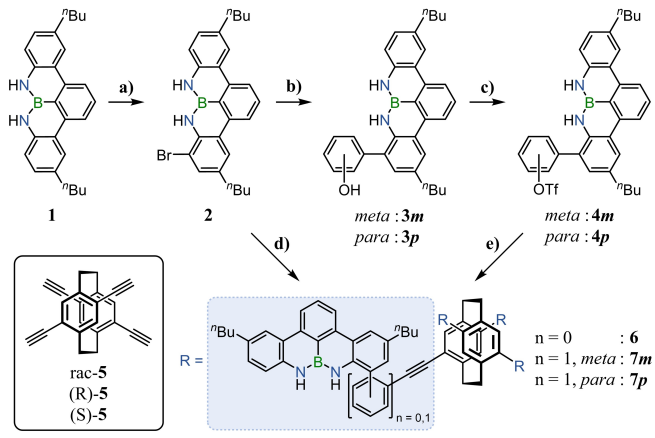

Scheme 1. Synthesis sequences toward **6**, **7*m*** and **7*p***. a) **1** (1.0 equiv), NBS (0.8 equiv), MeCN/CH_2Cl_2/$CHCl_3$ 1:4:4 *v/v*, 0 °C to RT, 12 h, 52%; b) **2** (1.0 equiv), hydroxyphenylboronic acid pinacol ester (1.4 equiv), $Pd(PPh_3)_4$ (10 mol%), 2 M K_2CO_3 (4.0 equiv), THF, reflux, 40 h, 86–99%; c) **3** (1.0 equiv), Tf_2O (2.4 equiv), pyridine (10.3 equiv), CH_2Cl_2, 0 °C to RT, 2 h, 89%; d) **5** (1.0 equiv), **2** (4.4 equiv), CuI (22 mol%), $Pd_2(dba)_3$ (11 mol%), $(t\text{-Bu})_3PH \cdot BF_4$ (44 mol%), THF/Et_3N (1:1 *v/v*), 50 °C, 18 h, 79–82%. e) **5** (1.0 equiv), **4** (4.4 equiv), CuI (20 mol%), $PdCl_2$(dppf) (20 mol%), THF/Et_3N (1:1 *v/v*), 50 °C, 18 h, 61–64%.

Results and Discussion

Synthesis

We started the synthesis of the target molecules with the bromination of commercially available [2.2]paracyclophane to 4,7,12,15-tetrabromo[2.2]PCP,[40] followed by a modification of the procedure of Hopf *et al.*[41] to obtain 4,7,12,15-tetra(trimethylsilylethynyl)[2.2]PCP by Sonogashira coupling with trimethylsilylacetylene. Deviating from the literature procedure of Hopf *et al.*,[41] we used CuI/$Pd_2(dba)_3$ as catalysts with $(t\text{Bu})_3PH \cdot BF_4$ as co-ligand instead of CuI/$Pd(PPh_3)_4$, resulting in higher yield (86% compared to 45%) and the formation of fewer side-products. In the next synthesis step, the TMS groups are quantitatively cleaved off with K_2CO_3 to give *rac*-**5**. For enantiopure (*R*)-**5** and (*S*)-**5**, we followed Morisaki *et al.* who developed a six-step synthesis starting from 4,7,12,15-tetrabromo[2.2]PCP to obtain the enantiomers in 14% yield with *ee* > 99.5%.[42] We obtained (*R*)-**5** and (*S*)-**5** with yields of 17 and 20%, respectively, and an *ee* ≥ 99.9% as estimated through HPLC-MS experiments of the diastereomeric camphanic ester intermediates. For the final step, the terminal ethynyl groups of *rac*-**5**, (*R*)-**5**, or (*S*)-**5** are coupled with 1-bromo-NBN-benzo[*f*,*g*]tetracene **2** reported recently by our group[43] in a fourfold palladium-catalyzed cross-coupling reaction, again using CuI/$Pd_2(dba)_3$/$(t\text{Bu})_3PH \cdot BF_4$, to afford the desired products *rac*-**6** (82%), (*R*)-**6** (79%), and (*S*)-**6** (80%).

For comparison, the structure of compound **6** was extended by *meta*- and *para*-phenylene linkers between the PCP core and NBN pendants to give new materials *m*-Ph-NBN-PCP **7*m*** and *p*-Ph-NBN-PCP **7*p*** (Scheme 1). Synthesis attempts of the *ortho*-phenylene linked derivative were unsuccessful, presumably due to steric constraints. For the synthesis of phenylene-linked derivatives **7*m*** and **7*p***, compound **2** was treated with commercially available 2- or 3-hydroxyphenylboronic acid pinacol ester in a Suzuki coupling reaction to obtain **3*m*** in 99% and **3*p*** in 86% yield. Triflation of **3*m*** and **3*p*** yielded the desired precursors **4*m*** and **4*p*** (89% each). The final steps were performed in a fashion similar to compound **6** by Sonogashira coupling with tetraethynyl[2.2]PCPs *rac*-**5**, (*R*)-**5**, and (*S*)-**5**, to afford the desired products *rac*-**7*m*** (63%), (*R*)-**7*m*** (64%), (*S*)-**7*m*** (61%), *rac*-**7*p*** (61%), (*R*)-**7*p*** (62%), and (*S*)-**7*p*** (61%).

The synthesis routes presented herein provide access to **6** from **2** and 4,7,12,15-tetrabromo[2.2]PCP with overall yields of 70% over three steps for the racemic compound *rac*-**6** and 14 and 16% over seven steps for (*R*)-**6** and (*S*)-**6**, respectively. Phenylene-linked derivatives **7*m*** and **7*p*** can be obtained from **2** and 4,7,12,15-tetrabromo[2.2]PCP in six steps for *rac*-**7*m*** (46% overall yield) and *rac*-**7*p*** (40%) and in nine steps for (*R*)-**7*m*** (9%), (*S*)-**7*m*** (11%), (*R*)-**7*m*** (8%), and (*S*)-**7*p*** (9%), respectively. The novel compounds **6**, **7*m***, and **7*p*** were fully characterized by multinuclear (^1H, ^{13}C, ^{11}B) and correlated NMR spectroscopy

© 2021 The Authors. Chemistry - A European Journal published by Wiley-VCH GmbH

(H,H COSY, HSQC, HMBC), as well as by high-resolution mass spectrometry.

Optical properties

The UV/Vis spectrum of **6** in CH_2Cl_2 shows three main absorption features in the regions of 230–290, 310–380, and 400–475 nm (Figure 1). Comparison with absorption spectra of the subunits **1** and *rac*-**5** indicates considerable changes due to coupling of the building blocks, most notably the rise of the most longwave absorption bands around 400–475 nm with maximum at 446 nm. Note that the related molar extinction coefficients of **6** are particularly large with $\varepsilon_{251\,nm}$ = 204 000 $M^{-1}cm^{-1}$, $\varepsilon_{359\,nm}$ = 86 300 $M^{-1}cm^{-1}$, and $\varepsilon_{446\,nm}$ = 81 700 $M^{-1}cm^{-1}$. For all three samples of **6** – racemic and enantiopure – identical spectra were recorded, thus hinting towards no significant aggregation in solution. This is in agreement with additional aggregation experiments of solutions of *rac*-**6** ranging from $c = 2.0\times10^{-6}$ M up to $c = 1.0\times10^{-3}$ M, which show that the UV/Vis spectra are unchanged in the concentration range investigated (Figure S50 in the Supporting Information).

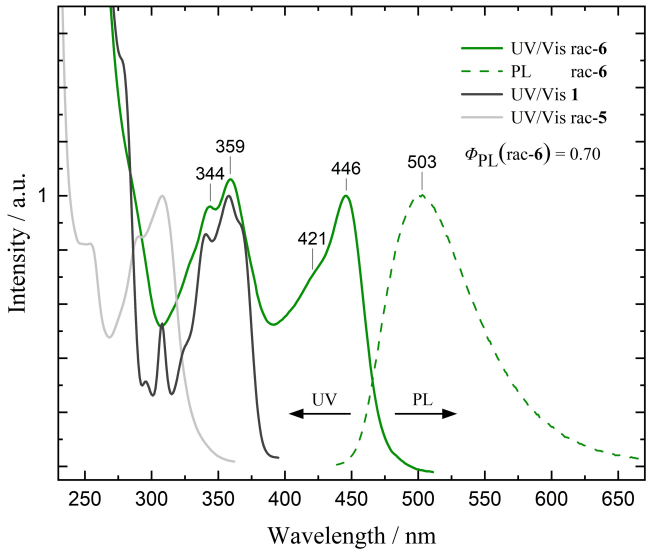

Figure 1. Normalized UV/Vis absorption spectra of *rac*-**6**, *rac*-**5** and **1** (2×10^{-6} M in CH_2Cl_2, 293 K) and emission spectrum of *rac*-**6** (λ_{ex} = 345 nm, 2×10^{-6} M in CH_2Cl_2, 293 K) with PL quantum yield Φ_{PL} of **6**. All spectra are normalized to the respective lowest energy transition.

The emission spectrum of compound **6** (Figure 1) in CH_2Cl_2, recorded with an excitation wavelength of 345 nm, consists of one broad emission band with maximum at 503 nm without any resolved vibrational fine structure. The unstructured PL spectrum is indicative of an excited state with strong intramolecular charge transfer character. A rather large Stokes shift of 2460 cm^{-1} in CH_2Cl_2 was observed. Emission spectra recorded in THF show an identical emission band with λ_{max} = 498 nm, but for a sample in toluene a far narrower and more hypsochromically shifted band with λ_{max} = 474 nm is observed with a Stokes shift of 1530 cm^{-1} (Figure S49). As charge-separated excited states are less stabilized in nonpolar solvents, the higher energy of the emission band observed in toluene compared to more polar solvents indicates that the emitting electronic state of compound **6** is (at least partially) charge separated. Following Kasha's rule, the position of the observed structureless emission band in either CH_2Cl_2, THF, or toluene is independent of excitation wavelength. The PL quantum yield of **6** was measured to be Φ_{PL} = 0.70 for both racemic and enantiopure samples, greatly outperforming pristine NBN-benzo[*f*,*g*]tetracene (Φ_{PL} = 0.24).[39] Combined with the high extinction coefficients, this certifies excellent optical properties of the compound, considering possible applications in optoelectronics. A commonly employed metric to assess the performance of fluorophores is the PL brightness *B*,[44] defined as the product of the molar extinction coefficient at the excitation wavelength and the PL quantum yield.[15] Applied to *rac*-**6**, a brightness of 5.5×10^4 $M^{-1}cm^{-1}$ (λ_{ex} = 345 nm) is determined (Table 1), placing it close to very bright fluorophores such as fluorescein (6.3×10^4 $M^{-1}cm^{-1}$ in 0.1 M NaOH, λ_{ex} = 491 nm).[44]

Compounds *rac*-**7*m*** and *rac*-**7*p*** were investigated in a similar fashion (Figure 2). Most noticeably, both phenylene linked derivatives are lacking the most longwave absorption features around 400–475 nm observed in *rac*-**6**. This suggests a lack of conjugation between the PCP and the NBN aromatic system in the ground state. However, the detected emission bands in CH_2Cl_2 are very much comparable within all three derivatives with λ_{max} (*rac*-**6**) = 503 nm, λ_{max} (*rac*-**7*m***) = 515 nm, and λ_{max} (*rac*-**7*p***) = 499 nm, although the quantum yields are considerably lower at Φ_{PL} = 0.014 and 0.45 for *rac*-**7*m*** and *rac*-**7*p***, respectively. One reason for the differing quantum yields might be the higher structural flexibility of the phenylene linked compounds as compared to the acetylene linked compound, thereby opening up nonradiative relaxation pathways of the excited states. The ability for large amplitude motions can facilitate access to a conical intersection,[45] effectively lowering

Table 1. Optical properties of *rac*-**6**, *rac*-**7*m*** and *rac*-**7*p***.

	UV/Vis[a] λ_{max} [nm] (ε [10^5 $M^{-1}cm^{-1}$])	PL[b] λ_{max} [nm]	τ[c] [ns] (rel. ampl. [%])	χ^2[d]	Φ_{PL}[e]	B[f] [10^3 $M^{-1}cm^{-1}$]
rac-**6**	251 (2.04), 359 (0.86), 446 (0.82)	503	3.34 (24), 5.01 (76)	1.07	0.70	55
rac-**7*m***	252 (2.91), 360 (1.24), 375 (1.21)	515	3.03 (36), 11.3 (64)	1.11	0.014	1.4
rac-**7*p***	252 (2.67), 360 (1.23), 379 (1.23)	499	2.94 (29), 6.32 (71)	1.10	0.45	48

[a] In CH_2Cl_2 (2×10^{-6} M, 293 K). [b] In CH_2Cl_2 (2×10^{-6} M, 293 K), excited at λ_{ex} = 345 nm. [c] Luminescence lifetimes. [d] PL decay curves were best fitted to bi-exponential equations. [e] PL quantum yield. [f] Brightness[44] $B = \varepsilon_\lambda \times \Phi_{PL}$ at the excitation wavelength λ_{ex} = 345 nm.

© 2021 The Authors. Chemistry - A European Journal published by Wiley-VCH GmbH

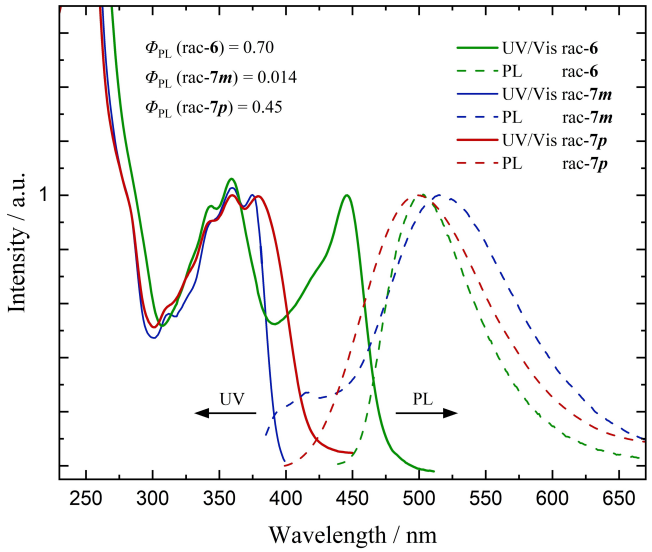

Figure 2. Normalized UV/Vis absorption and emission spectra (λ_{ex} = 345 nm) of freshly prepared solutions of *rac*-**6**, *rac*-**7m**, *rac*-**7p** (2×10^{-6} M in CH_2Cl_2, 293 K) with PL quantum yields Φ_{PL}. All spectra are normalized to the respective lowest energy transition.

the PL quantum yields.[46] Especially the *meta* phenylene linker leads to rather effective quenching of the emission. The observed Stokes shifts for the compounds with phenylene linkers are considerably higher (*rac*-**7m** 7250 cm^{-1}, *rac*-**7p** 6350 cm^{-1}) than the Stokes shift of 2460 cm^{-1} determined for *rac*-**6**.

Much to our regret, both *rac*-**7m** and *rac*-**7p** undergo rapid photoinduced decomposition in oxygen-free solutions, hampering not only easy handling but also accurate optical measurements of the pure compounds. Within the timespan of recording photoluminescence spectra, *rac*-**7m** forms unstable luminescent photoproducts ($\lambda_{max,em}$ = 417 nm), whereas *rac*-**7p** quickly loses emission intensity without the rise of new bands. Neither of these findings were observed for compound **6**. Further investigations by irradiation of deoxygenated samples with a laboratory grade UV lamp (λ = 366 nm, 2×6 W) confirmed a much higher stability of *rac*-**6** (4% loss of integrated intensity after 45 min) compared to *rac*-**7m** (loss of 54%) and *rac*-**7p** (complete vanishing of initial emission band) (Figure S53). Considering photolability, further chiroptical and computational studies were pursued only for the most promising compound **6**.

Computation

To further investigate the optical properties, computational studies were performed for **6′** (*R* isomer, replacing the *n*-butyl groups by hydrogen atoms for simplicity) at the TPSS-D3(BJ)/def2-QZVP level of theory (see the Supporting Information for details). Rotation about the C–C single bonds that link the NBN units to the PCP core provides in principle access to a number of conformers of **6′**. We found that the rotamer of D_2 point group symmetry is lowest in energy. Within this isomer the π–π overlap between the pairs of NBN building blocks, and consequently London dispersion interaction, is maximized. The distance between the boron atoms is 3.228 Å in this isomer (Figure 3b). The importance of the latter attraction is vividly seen in the relative energies of the rotamers: while all are within 1 kcal mol^{-1} in energy without the dispersion correction (D3(BJ)), the D_2 isomer turns more stable in energy by 18, 13, and 7 kcal mol^{-1} than C_1 and C_2 symmetry isomers with a reduced degree of π–π overlap (see Figure S62 for structures of the higher lying rotamers). As the energy differences are so large, the energetically higher lying isomers will not be populated significantly at room temperature. This is confirmed by variable temperature NMR experiments of *rac*-**6** (Figure S33) that present only one set of resonances in the temperature range monitored (218–318 K). Although the chemical shifts of

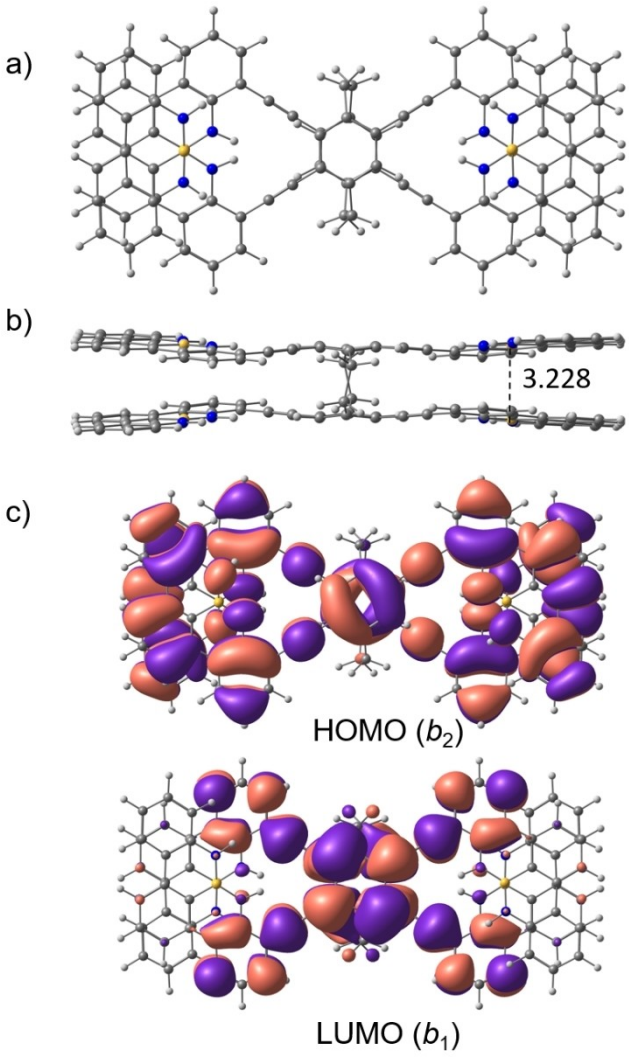

Figure 3. a) Top and b) side views of the structure of the D_2 isomer of **6′** (*n*-butyl groups replaced by H) computed at the TPSS-D3(BJ)/def2-QZVP level of theory. The boron–boron distance is given in Å. c) HOMO and LUMO (contour value 0.01) computed at the RHF/def2-TZVP//TPSS-D3(BJ)/def2-QZVP level of theory. The irreducible representations of the orbitals in the D_2 point group are given in parentheses.

© 2021 The Authors. Chemistry - A European Journal published by Wiley-VCH GmbH

some signals change greatly with temperature, no splitting of signals could be observed that would hint towards a dynamic equilibrium of multiple conformers. Hence, only the D_2 rotamer was investigated further.

The energy of excited states was computed using the wavefunction based ADC(2) level of theory with the def2-TZVP basis set for four states each of B_1, B_2, and B_3 symmetry. We chose this computationally demanding method as it was found to perform very well for $\pi\rightarrow\pi^*$ excitations and charge-transfer states.[47,48] The lowest energy transition ($1^1A\rightarrow1^1B_3$) to S_1 is computed to be at 426 nm with a very large oscillator strength ($f=1.373$). The 1^1B_2 (415 nm) and 1^1B_1 (393 nm) states correspond to S_2 and S_3, respectively, and transitions to these states have very small oscillator strengths ($f=0.026$ and 0.002, respectively). Hence, the absorption band observed at $\lambda_{max}=$ 446 nm is assigned to arise from the $S_0\rightarrow S_1$ transition that is dominated (80%) by an electronic excitation of one electron from HOMO to LUMO (Figure 3c). The HOMO is distributed over the entire molecule with large coefficients on the NBN subunits, while the LUMO is primarily located on the central [2.2]PCP core. This suggests that the electronic transition has some charge transfer character and shows that the electronic interaction of NBN and PCP subunits results in a strong broad band observed in the absorption spectrum that is absent for either building block.

As an alternative to the ADC(2) method, we employed time-dependent density functional theory (TD-DFT) for analysis of the optical spectrum using the def2-TZVP basis set. In view of the charge transfer character, the long-range corrected functionals CAM-B3LYP-D3(BJ)[49] and ωB97XD[50] as well as the multi-parameter hybrid meta-GGA functional M06-2X[51] were chosen. While the latter considers dispersion interactions to some degree by construction, the other two functionals use Grimme's[52–54] dispersion corrections. Note that the description of dispersion interaction between the NBN subunits of **6**′ in the excited states is problematic for TD-DFT as the dispersion corrections were derived for electronic ground states.[55] All functionals place the 1^1B_2 state slightly below (0.01–0.05 eV) the 1^1B_3 state. As the oscillator strength of the 1^1B_2 transition is very small, the computed absorption spectrum is unaffected by this change of the order of excited states. Indeed, the spectrum obtained at the M06-2X level is in good agreement with experiment (Figure S64).

Chiroptical properties

To gain an insight into the chiroptical properties in the ground and excited states of **6**, enantiopure samples were investigated by ECD and CPL spectroscopy. Intense and mirror image Cotton effects were observed in the ECD spectra of (*R*)-**6** and (*S*)-**6** (Figure 4a). The computed spectrum (M06-2X/def2-TZVP, Figure S65) is in good agreement with the experimental one in terms of sign, sequence, and magnitude of bands, which is in support of considering only the D_2 conformer of **6**′. A value of $[\theta]=\pm6.1\times10^5$ deg cm^2 dmol^{-1} was obtained for the molar ellipticity at $\lambda=232$ nm. The absorption dissymmetry factors

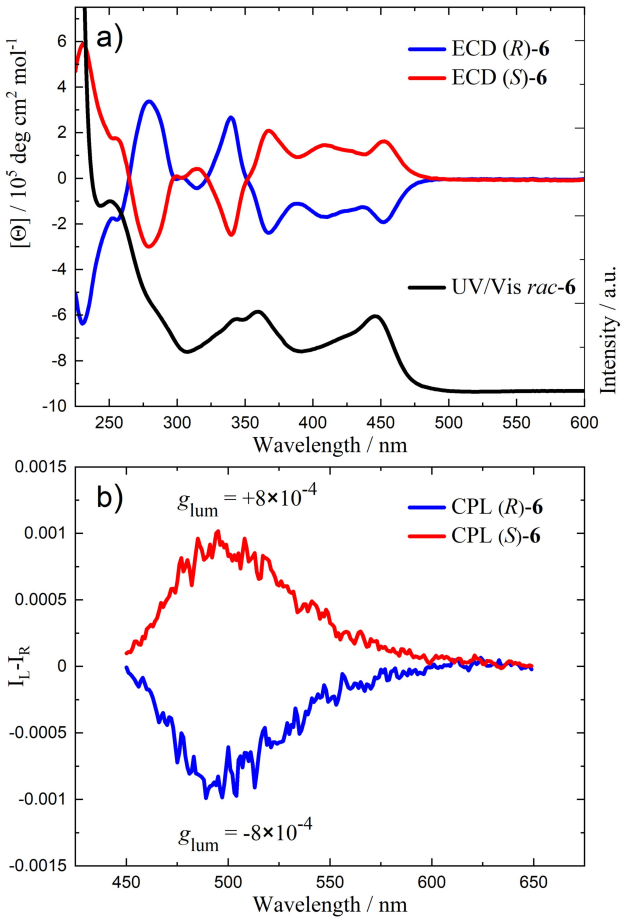

Figure 4. Chiroptical data of (*R*)-**6** and (*S*)-**6**: a) ECD spectra (6.5×10^{-5} M, CH_2Cl_2, 293 K) with UV/Vis absorption spectrum. b) CPL spectra ($\lambda_{ex}=365$ nm, 2.0×10^{-4} M, CH_2Cl_2, 293 K).

(g_{abs}) calculated for the most red-shifted Cotton effect in the ECD spectrum at 451 nm are $+8\times10^{-4}$ and -8×10^{-4} for (*S*)-**6** and (*R*)-**6**, respectively. The specific rotation $[\alpha]^{20}_{589}$ ($c=0.50$, $CHCl_3$) was determined to be +1192° for (*R*)-**6** and −1189° for (*S*)-**6**.

The samples display clear mirror image CPL bands (Figure 4b) centered around 500 nm (positive for (*S*)-**6** and negative for (*R*)-**6**), closely retracing the luminescence spectrum. The g_{lum} values calculated for (*S*)-**6** and (*R*)-**6** are $+8\times10^{-4}$ and -8×10^{-4}, respectively (Table 2). With the molar extinction coefficient at excitation wavelength ε_λ, the PL quantum yield Φ_{PL}, and the

Table 2. Chiroptical properties of (*R*)-**6** and (*S*)-**6**

	g_{abs} [a]	g_{lum} [b]	B_{CPL} [c] [M^{-1} cm^{-1}]	$[\alpha]^{20}_{589}$ [d] [°]
(*R*)-**6**	-8×10^{-4}	-8×10^{-4}	21.9	+1192
(*S*)-**6**	$+8\times10^{-4}$	$+8\times10^{-4}$	21.9	−1189

[a] $g_{abs}=\Delta\varepsilon/\varepsilon$, in CH_2Cl_2 (2×10^{-4} M, 293 K) calculated at 451 nm. [b] $g_{lum}=2(I_L-I_R)/(I_L+I_R)$, in CH_2Cl_2 (4.5×10^{-5} M, 293 K), excited at $\lambda_{ex}=365$ nm. [c] Brightness for CPL[15] $B_{CPL}=\varepsilon_\lambda\times\Phi_{PL}\times|g_{lum}|/2$ at $\lambda_{ex}=365$ nm. [d] $[\alpha]^{20}_{589}=\alpha_{obs}/(cl)$, in $CHCl_3$ (0.500 g mL^{-1}, 293 K).

© 2021 The Authors. Chemistry - A European Journal published by Wiley-VCH GmbH

dissymmetry factor g_{lum}, a circular polarized brightness B_{CPL} of 21.9 $M^{-1}cm^{-1}$ can be determined for compound **6** via $B_{CPL} = \varepsilon_\lambda \times \Phi_{PL} \times |g_{lum}|/2$.[56] Typical B_{CPL} obtained for CPL-active [2.2]PCPs are in the range of 5.2–333 $M^{-1}cm^{-1}$ with a median of 31.9 $M^{-1}cm^{-1}$.[15] The g_{lum} versus wavelength plot (Figure S54) shows that the dissymmetry factor g_{lum} is constant throughout the emission band, which is compatible with a single transition responsible for the emission spectrum. It is worth noting that these values agree in sign and magnitude with the absorption dissymmetry factors (g_{abs}) calculated for the most red-shifted Cotton effect in the ECD spectrum (451 nm). This usually indicates that the geometries of the ground and the emitting excited states are relatively similar. The nearby NBN-benzo[*f*,*g*]tetracene units seen in Figure 3 may suggest that emission originates from a diffuse state adjoining two closely stacked chromophores, that is, a sort of intramolecular excimer. This event can be ruled out by the constant g_{lum} observed above and by the similarity of g_{abs} and g_{lum}.

Although rare, TD-DFT computations of CPL dissymmetry factors have been reported several times, most recently by Kubo *et al.*[57–62] Using the values for the transition electronic dipole moment (TEDM) μ, the transition magnetic dipole moment (TMDM) m, and the angle $\theta_{\mu,m}$ between TEDM and TMDM computed at the optimized structure of the emitting S_1 state, a theoretical value of $g_{lum,calcd.}$ can be obtained with Equation (1), where R is the rotatory strength of the emitting transition.[57]

$$g_{lum,calcd.} = \frac{I_L - I_R}{\frac{1}{2}(I_L + I_R)} = \frac{4|\mu||m|\cos\theta_{\mu,m}}{|\mu|^2 + |m|^2} = \frac{4R}{|\mu|^2 + |m|^2} \quad (1)$$

We applied this approach to compute $g_{lum,calcd.}$ of (*R*)-**6′** using a number of functionals (Table 3). As stated above, the description of London dispersion interactions in the excited state is problematic for these functionals. However, the good agreement between experiment and theory for the absorption spectrum obtained with M06-2X encouraged us to also compute $g_{lum,calcd.}$ using this and other functionals. Note that during geometry optimization the order of the energy of electronic states 1^1B_3 and 1^1B_2 switches. Hence, the geometry optimized S_1 state corresponds for all functionals to 1^1B_3 with large oscillator strength, in agreement with the observation of bright luminescence. We used CAM-B3LYP to take advantage of the improved charge transfer excitation representation of the Coulomb-attenuating method.[49] A very low $g_{lum,calcd.}$ of $+2.48\times10^{-5}$ was obtained, mainly because the angle $\theta_{\mu,m}$ between TEDM and TMDM is close to 90°. With D3(BJ) correction, $\theta_{\mu,m}$ is increased to 93.73° and consequently the absolute value of $g_{lum,calcd.}$ becomes larger. Also, the sign switches from positive to negative (-4.16×10^{-4}), agreeing with the experimental value of (*R*)-**6**. The ωB97XD functional arrives at a similar value (-3.50×10^{-4}). The result that is closest to the experimentally measured $g_{lum} = -8\times10^{-4}$ was obtained with M06-2X (-7.13×10^{-4}).

To test the performance of M06-2X for the g_{lum} computation of similar systems, the *R* isomers of the known compounds (*R*)-tetra(phenylethynyl)[2.2]PCP ((*R*)-Ph-PCP), (*R*)-tetra(naphthylethynyl)[2.2]PCP ((*R*)-Naph-PCP), and (*R*)-tetra(anthracenylethynyl)[2.2]PCP ((*R*)-Anth-PCP) were computed and the theoretical values were compared with the reported[63] experimental ones (Table 4).

Given that these computations are performed for isolated molecules without consideration of solvation effects and that a correct representation of the dispersion interactions in the excited state is not guaranteed in M06-2X (in fact in none of the currently available functionals), the calculated $g_{lum,calcd.}$ are surprisingly close to the experimental values, most certainly in the right magnitude. These results demonstrate the potential of g_{lum} calculations for material design of CPL emitters, and we encourage further research.

Electrochemical studies

In contrast to optical methods, which deal with ground and excited states of the molecules, electrochemical techniques probe the electron transfer properties, that is, processes that involve different redox states remaining in the electronic ground state. Thus, *rac*-**6** and its subunits **1** and *rac*-**5** were investigated by cyclic voltammetry (CV) using a Pt or a glassy carbon (GC) working electrode in a CH_2Cl_2/0.1 M NBu_4PF_6 electrolyte at various scan rates ($0.02 \le v \le 10\ V\,s^{-1}$) and bulk concentrations c^0 in the mM range.

The paracyclophane unit *rac*-**5** does not show any CV signal in the potential range between +1.093 and −2.607 V (all potentials are reported vs. the ferrocene/ferricinium standard redox couple).[64] This covers potentials down to the negative potential limit of the electrochemical window and extends even more positive than the positive potentials used for oxidation of **1** and *rac*-**6** (see below). The absence of redox processes is in accordance with the relatively high potentials reported for

Table 3. TD-DFT computations of $g_{lum,calcd.}$ for compound (*R*)-**6′**, compared with the experimental value. All computations utilize the def2-SV(P) basis set.

Method	$\|\mu\|$ [10^{-20} esu cm]	$\|m\|$ [10^{-20} erg G^{-1}]	$\theta_{\mu,m}$	$g_{lum,calcd}$ [10^{-4}]
CAM-B3LYP	1125	1.697	89.76	+0.248
CAM-B3LYP-D3(BJ)	1109	1.773	93.73	−4.16
ωB97XD	1096	1.862	92.95	−3.50
M06-2X	1106	1.771	96.39	−7.13
experimental for (*R*)-**6**				−8

Table 4. Comparison of experimental and computed (M06-2X/def2-SV(P)) g_{lum} values.

Compound	$g_{lum,calcd.}$ [10^{-4}]	g_{lum} [10^{-4}]
(*R*)-**6**	−7.13[a]	−8
(*R*)-Ph-PCP	−20.1	−12[63]
(*R*)-Naph-PCP	−17.7	−17[63]
(*R*)-Anth-PCP	−13.6[a]	−4[63]

[a] The values computed for (*R*)-**6** and (*R*)-Anth-PCP were obtained with the respective model compounds (*R*)-**6′** and (*R*)-Anth-PCP′ that had the *n*-butyl groups replaced by hydrogen atoms.

© 2021 The Authors. Chemistry - A European Journal published by Wiley-VCH GmbH

reduction[65,66] or oxidation[67] of cyclophane-type hydrocarbons without electronically active substituents.

On the other hand, bis-*n*-butyl substituted NBN-benzo[*f,g*]tetracene **1** is oxidized in a chemically reversible one-electron transfer reaction featuring peaks I(**1**) and II(**1**) at $E^0 = +0.444 \pm 0.002$ V with a peak current ratio $I_p^{red}/I_p^{ox} = 0.98 \pm 0.01$ (see Figure 5a for the voltammogram at $v = 0.2\ V\,s^{-1}$ and the Supporting Information for current-potential curves at other scan rates). The process is diffusion controlled and electrochemically reversible (peak current proportional to the square root of the scan rate; $\Delta E_p = 83 \pm 8$ mV, somewhat increased above the ideal value of 58 mV) up to $v = 0.5\ V\,s^{-1}$ with a transition to quasireversibility (increasing ΔE_p with increasing v) at higher scan rates. A combination of steady-state microelectrode and chronoamperometric data[68] allows the determination of the diffusion coefficient ($D = 1.38 \pm 0.02 \times 10^{-5}\ cm^2\,s^{-1}$) and the number of transferred electrons per molecule $n = 0.89 \pm 0.01$, consistent with the one-electron oxidation of **1** to its radical cation. Voltammograms extending to more positive potentials show a second, chemically irreversible oxidation peak, which was, however, not analyzed in detail. No reduction signal of **1** could be observed at potentials extending down to the negative limit of the electrochemical window.

The cyclic voltammogram of *rac*-**6**, which combines both subunits, in the positive potential range shows two peaks I(*rac*-**6**) and II(*rac*-**6**) for oxidation and an associated reduction (Figure 5b). The voltammetric signal is slightly distorted by adsorption of the oxidation product, as indicated by the pointed shape of the reduction peak and an increased peak current ratio $I_p^{red}/I_p^{ox} > 1$, in particular at low scan rates, where also ΔE_p decreases significantly below 58 mV. At larger v, the value of ΔE_p increases, again indicating the transition to a quasi-reversible electron transfer. Scans to more positive potentials reveal two additional oxidation signals. However, under these conditions the adsorption phenomena become prohibitive for further analysis of the voltammograms, and these data are not considered further. The number of electrons transferred in peak I(*rac*-**6**) is determined as $n = 2.3 \pm 0.2$ ($D = 5.8 \pm 0.4 \times 10^{-6}\ cm^2\,s^{-1}$). The two electron transfer steps are not resolved in the voltammograms, and individual E^0 cannot be estimated. The signal is characterized by a midpoint potential $\bar{E} = +0.309 \pm 0.02$ V close to the oxidation formal potential of subunit **1**, where $\bar{E}$ is the mean value of E_p(I(*rac*-**6**)) and E_p(II(*rac*-**6**)). The shift to less positive potentials as compared to **1** is explained by the inductive effect of the ethynyl linkers and possibly by the larger extension of the π-system, stabilizing the product.

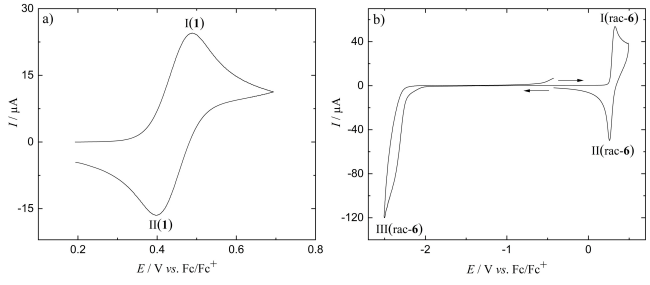

Figure 5. Cyclic voltammograms in CH_2Cl_2/0.1 M NBu_4PF_6 at $v = 0.2$ V/s of a) **1**, Pt electrode, $c^0 = 1.2$ mM. b) *rac*-**6**, GC electrode, $c^0 = 1.12$ mM.

The nature of the two-electron oxidation in peaks I/II of *rac*-**6** was investigated computationally. Vertical (diabatic) ionization is not sufficient to describe electron transfers between a molecule in solution and an electrode owing to the comparably slow time scale of charge transfer.[69] Instead, adiabatic ionization energies have to be determined that are defined as the difference between the zero-point energy corrected total energies of the two respective redox species. Extended research by Isegawa *et al.* proved that the hybrid meta-GGA DFT functional M06-2X is well suited for calculations of ionization energies with a mean unsigned error of around 0.1 eV.[70] We assume that the neutral compound is oxidized first to a radical cation and then to a diradical dication. For the latter, we consider the triplet state for computational simplicity. The geometries of neutral **6′**, radical cation $\mathbf{6'}^{+}$, and diradical dication $\mathbf{6'}^{2+}$ were optimized at the TPSS-D3(BJ)/def2-TZVP level followed by single-point energy computation at the M06-2X/def2-TZVP level of theory. The solvation model based on density (SMD)[71] was used to simulate the solvation energies in CH_2Cl_2. From the computed harmonic vibrational frequencies, the zero-point energy corrected energy difference ΔE_{ZPE}, the enthalpy ΔH^0 (at 298 K) and the Gibbs free energy ΔG^0 (at 298 K) can be calculated (TPSS-D3(BJ)/def2-TZVP) for each ionization state (Table 5). As a result, a small energy difference $\Delta\Delta G^0$ of +0.12 eV between the first and second oxidation step of **6′** is obtained. The spin density distribution (Figure S66) strongly differs between the redox states: while it is mainly located on the central cyclophane unit and the directly surrounding atoms in the radical cation, it is mostly shifted to the NBN substituents in the diradical dication.

Some necessary simplifications have to be considered when attempting to relate the calculated energy difference to the corresponding difference between two redox potentials associated with the oxidation steps of *rac*-**6**: the replacement of butyl groups with hydrogen atoms to reduce convergence and conformational issues and the neglect of supporting electrolyte in the solvation model. The electrolyte is expected to increase the polarity, which in turn should preferentially stabilize the dication and result in a decreased ionization potential associated with its formation. Still the computed small value of $\Delta\Delta G^0$ is in agreement with the absence of a noticeable peak splitting in the voltammograms. For paracyclophanes with multiple redox centers attached by both ethynyl and vinyl linkers only

Table 5. Zero-point energy corrected electronic energy ΔE_{ZPE}, enthalpy ΔH^0 (at 298 K) and Gibbs free energy ΔG^0 (at 298 K) in solution (SMD method in CH_2Cl_2, M06-2X/def2-TZVP//TPSS-D3(BJ)/def2-TZVP) for the adiabatic oxidation steps of **6′** to the radical cation $\mathbf{6'}^{+}$ and the diradical dication $\mathbf{6'}^{2+}$.

Oxidation step	ΔE_{ZPE} [eV]	ΔH^0 [eV]	ΔG^0 [eV]
$\mathbf{6'} \rightarrow \mathbf{6'}^{+}$	5.76	5.74	5.75
$\mathbf{6'}^{+} \rightarrow \mathbf{6'}^{2+}$	5.89	5.89	5.87

© 2021 The Authors. Chemistry - A European Journal published by Wiley-VCH GmbH

small effects of interaction between the redox active groups have been reported,[72–74] resulting in overlapping peaks for the two subsequent electron transfers. An analogous situation must apply here.

The reduction of *rac*-**6** is chemically irreversible (III(*rac*-**6**), Figure 5b) without a reverse peak and superimposed on the current resulting from decomposition of the supporting electrolyte at the negative limit of the electrochemical window.

A HOMO-LUMO gap of $\approx$2.3 eV for *rac*-**6** is estimated as the difference between the onset potentials for the reduction in wave III(*rac*-**6**) and oxidation in peak I(*rac*-**6**).[75] This is lower than the optical and computational HOMO–LUMO gap of $\Delta E \approx 2.8$ eV. It should be noted, however, that although such estimations from CV data are common in the literature, the onset potential is only loosely defined as compared to, for example, a formal potential. There are also fundamental and practical differences between electrochemical potentials and orbital energies, which inevitably limits the reliability of such values.[69,76,77]

Conclusion

We have extended the class of multisubstituted [2.2]paracyclophanes for the first time by a BN-doped polycyclic aromatic hydrocarbon. Within the novel structures, four NBN-benzo[*f*,*g*]tetracenes are either directly coupled to the chiral PCP core via ethynyl linkers (compound **6**) or have an additional *m*- or *p*-phenylene spacer in between the PCP and the NBN building blocks (**7*m*** and **7*p***). Density functional computations indicate large London dispersion between the NBN units in a graphite-like layering with short distances between these moieties. Electrochemical studies of **6** and its subunits indicate a two-electron process for the first oxidation of **6**. Quantum-mechanical calculations of the first and second adiabatic ionization energies are in accordance with the assumption of two consecutive one-electron transfers leading to a radical cation and then a diradical dication. The small difference in the ionization energies is consistent with a small difference in formal potentials for the two steps that leads to a single voltammetric peak. While **6** proved to have high chemical stability in the presence of water, oxygen, and light, **7*m*** and **7*p*** undergo rapid photodegradation in solution. Formation of these large structures has an exceptional impact on the optical and chiroptical properties compared with either building block, mainly contributed to a significant charge transfer character of the transitions and intense chromophore coupling. ECD and CPL spectroscopy of **6** revealed a strong chiral environment in the ground and excited states with values of g_{abs} and g_{lum} of $\pm 8\times10^{-4}$. Quantum-mechanical computations were performed to obtain theoretical values of $g_{lum,calcd.}$ that match the experimental values. Combined with an excellent PL quantum yield Φ_{PL} of 0.70 and very high absorption coefficients ε of up to $2.04\times10^5\,M^{-1}cm^{-1}$, the novel compound **6** is a proficient chiral emitter.[15] These results suggest that the 3D arrangement evoked by the PCP scaffold, a combination of strong chromophore coupling through-space and through-bond, and a resulting CT character might lead to drastically improved (chir-)optical characteristics, even with chromophores that are lowly to moderately emissive as monomers. With this work, we could demonstrate that the combination of nonclassical chromophores like BN-doped polyaromatic hydrocarbons and a [2.2]PCP scaffold can be a promising approach for emergent highly luminescent CPL materials.

Acknowledgements

The authors acknowledge support by the state of Baden–Württemberg through bwHPC and the German Research Foundation (DFG) through grant no INST 40/467-1 FUGG (JUSTUS cluster). Open Access funding enabled and organized by Projekt DEAL.

Conflict of Interest

The authors declare no conflict of interest.

Data Availability Statement

The data that support the findings of this study are available in the supplementary material of this article.

Keywords: chirality · circularly polarized luminescence · computational chemistry · cyclophanes · electrochemistry

[1] O. L. Pavlenko, O. P. Dmytrenko, M. P. Kulish, V. A. Sendiuk, N. V. Obernikhina, Y. O. Prostota, O. D. Kachkovsky, L. A. Bulavin, *Electron Structure and Optical Properties of Conjugated Systems in Solutions, in International Conference Physics of Liquid Matter: Modern Problems of the Physics of Liquid Systems (Eds.:* L. A. Bulavin, L. Xu), Springer, Cham, **2019**, pp. 225–248.
[2] O. M. Opeyemi, H. Louis, C. I. Oparab, O. O. Funmilayo, T. O. Magu, *Adv. J. Chem. A* **2019**, *2*, 21–44.
[3] C. Wang, X. Zhang, W. Hu, *Chem. Soc. Rev.* **2020**, *49*, 653–670.
[4] Y. Mei, *Organic Transistor – Device Structure, Model and Applications, in Nanoelectronics* (Eds.: *B. K. Kaushik*), Elsevier, **2019**, pp. 115–129.
[5] C. Dyer-Smith, J. Nelson, *Organic Solar Cells, in Practical Handbook of Photovoltaics (Second Edition)* (Eds.: A. McEvoy, T. Markvart, L. Castaner), Academic Press, Cambridge, **2012**, pp. 543–569.
[6] M. Demelas, S. Lai, P. Cosseddu, A. Loi, M. Barbaro, A. Bonfiglio, *Chemical sensors using organic thin-film transistors (OTFTs), in Handbook of Flexible Organic Electronics* (Eds.: S. Logothetidis), Elsevier, **2015**, pp. 375–396.
[7] R. J. Martín-Palma, J. M. Martínez-Duart, *Novel Advanced Nanomaterials and Devices for Nanoelectronics and Photonics, in Nanotechnology for Microelectronics and Photonics (Second Edition)* (Eds.: R. J. Martín-Palma, J. M. Martínez-Duart), Elsevier, **2017**, pp. 243–263.
[8] D. Padula, Ö. H. Omar, T. Nematiaram, A. Troisi, *Energy Environ. Sci.* **2019**, *12*, 2412–2416.
[9] M. B. Smith, J. Michl, *Annu. Rev. Phys. Chem.* **2013**, *64*, 361–386.
[10] D. N. Congreve, J. Lee, N. J. Thompson, E. Hontz, S. R. Yost, P. D. Reusswig, M. E. Bahlke, S. Reineke, T. Van Voorhis, M. A. Baldo, *Science* **2013**, *340*, 334–337.
[11] D. L. Andrews, *Photonics, Vol. 1: Fundamentals of Photonics and Physics*, Wiley, Hoboken, **2015**, pp. 1–20.
[12] E. M. Sánchez-Carnerero, A. R. Agarrabeitia, F. Moreno, B. L. Maroto, G. Muller, M. J. Ortiz, S. de la Moya, *Chem. Eur. J.* **2015**, *21*, 13488–13500.
[13] H. G. Brittain, *Chirality* **1996**, *8*, 357–363.
[14] J. P. Riehl, F. S. Richardson, *Chem. Rev.* **1986**, *86*, 1–16.

© 2021 The Authors. Chemistry - A European Journal published by Wiley-VCH GmbH

[15] L. Arrico, L. Di Bari, F. Zinna, *Chem. Eur. J.* **2021**, *27*, 2920–2934.
[16] G. Longhi, E. Castiglioni, J. Koshoubu, G. Mazzeo, S. Abbate, *Chirality* **2016**, *28*, 696–707.
[17] J. Kumar, T. Nakashima, T. Kawai, *J. Phys. Chem. Lett.* **2015**, *6*, 3445–3452.
[18] M. Grell, D. D. C. Bradley, *Adv. Mater.* **1999**, *11*, 895–905.
[19] F. Vögtle, G. Hohner, *Top. Curr. Chem.* **1978**, *74*, 1–29.
[20] D. J. Cram, H. Steinberg, *J. Am. Chem. Soc.* **1951**, *73*, 5691–5704.
[21] C. J. Brown, *J. Chem. Soc.* **1953**, 3265–3270.
[22] Y. Morisaki, M. Gon, Y. Chujo, *J. Polym. Sci. Part A* **2013**, *51*, 2311–2316.
[23] M. Gon, Y. Morisaki, R. Sawada, Y. Chujo, *Chem. Eur. J.* **2016**, *22*, 2291–2298.
[24] Y. Morisaki, M. Gon, T. Sasamori, N. Tokitoh, Y. Chujo, *J. Am. Chem. Soc.* **2014**, *136*, 3350–3353.
[25] Y. Morisaki, Y. Chujo, *Bull. Chem. Soc. Jpn.* **2019**, *92*, 265–274.
[26] H. Maeda, M. Kameda, T. Hatakeyama, Y. Morisaki, *Polymer* **2018**, *10*, 1140.
[27] N. Sharma, E. Spuling, C. M. Mattern, W. Li, O. Fuhr, Y. Tsuchiya, C. Adachi, S. Bräse, I. D. W. Samuel, E. Zysman-Colman, *Chem. Sci.* **2019**, *10*, 6689–6696.
[28] M. Y. Zhang, X. Liang, D. N. Ni, D. H. Liu, Q. Peng, C. H. Zhao, *Org. Lett.* **2021**, *23*, 2–7.
[29] M. J. D. Bosdet, W. E. Piers, *Can. J. Chem.* **2009**, *87*, 8–29.
[30] Z. Liu, T. B. Marder, *Angew. Chem. Int. Ed.* **2008**, *47*, 242–244; *Angew. Chem.* **2008**, *120*, 248–250.
[31] P. G. Campbell, A. J. V. Marwitz, S.-Y. Liu, *Angew. Chem. Int. Ed.* **2012**, *51*, 6074–6092; *Angew. Chem.* **2012**, *124*, 6178–6197.
[32] M. Stępień, E. Gońka, M. Żyła, N. Sprutta, *Chem. Rev.* **2017**, *117*, 3479–3716.
[33] K. Matsui, S. Oda, K. Yoshiura, K. Nakajima, N. Yasuda, T. Hatakeyama, *J. Am. Chem. Soc.* **2018**, *140*, 1195–1198.
[34] X.-Y. Wang, J.-Y. Wang, J. Pei, *Chem. Eur. J.* **2015**, *21*, 3528–3539.
[35] D. Bonifazi, F. Fasano, M. M. Lorenzo-Garcia, D. Marinelli, H. Oubaha, J. Tasseroul, *Chem. Commun.* **2015**, *51*, 15222–15236.
[36] H. Helten, *Chem. Eur. J.* **2016**, *22*, 12972–12982.
[37] J. Y. Wang, J. Pei, *Chin. Chem. Lett.* **2016**, *27*, 1139–1146.
[38] Z. Sun, C. Yi, Q. Liang, C. Bingi, W. Zhu, P. Qiang, D. Wu, F. Zhang, *Org. Lett.* **2020**, *22*, 209–213.
[39] X. Wang, F. Zhang, K. S. Schellhammer, P. Machata, F. Ortmann, G. Cuniberti, Y. Fu, J. Hunger, R. Tang, A. A. Popov, R. Berger, K. Müllen, X. Feng, *J. Am. Chem. Soc.* **2016**, *138*, 11606–11615.
[40] B. König, B. Knieriem, A. De Meijere, *Chem. Ber.* **1993**, *126*, 1643–1650.
[41] L. Bondarenko, I. Dix, H. Hinrichs, H. Hopf, *Synth.* **2004**, *2004*, 2751–2759.
[42] Y. Morisaki, M. Gon, T. Sasamori, N. Tokitoh, Y. Chujo, *J. Am. Chem. Soc.* **2014**, *136*, 3350–3353.
[43] M. Fingerle, S. Stocker, H. F. Bettinger, *Synth.* **2019**, *51*, 4147–4152.
[44] K. L. Wong, J. C. G. Bünzli, P. A. Tanner, *J. Lumin.* **2020**, *224*, 117256.
[45] R. Crespo-Otero, Q. Li, L. Blancafort, *Chem. Asian J.* **2019**, *14*, 700–714.
[46] J. Gierschner, J. Shi, B. Milián-Medina, D. Roca-Sanjuán, S. Varghese, S. Park, *Adv. Opt. Mater.* **2021**, *9*, 2002251.
[47] H. Li, R. Nieman, A. J. A. Aquino, H. Lischka, S. Tretiak, *J. Chem. Theory Comput.* **2014**, *10*, 3280–3289.
[48] M. Véril, A. Scemama, M. Caffarel, F. Lipparini, M. Boggio-Pasqua, D. Jacquemin, P.-F. Loos, *WIREs Comput. Mol. Sci.* **2021**, *11*, e1517.
[49] T. Yanai, D. P. Tew, N. C. Handy, *Chem. Phys. Lett.* **2004**, *393*, 51–57.
[50] J. Da Chai, M. Head-Gordon, *Phys. Chem. Chem. Phys.* **2008**, *10*, 6615–6620.
[51] Y. Zhao, D. G. Truhlar, *Theor. Chem. Acc.* **2008**, *120*, 215–241.
[52] S. Grimme, *J. Comput. Chem.* **2006**, *27*, 1787–1799.
[53] S. Grimme, J. Antony, S. Ehrlich, H. Krieg, *J. Chem. Phys.* **2010**, *132*, 154104.
[54] S. Grimme, S. Ehrlich, L. Goerigk, *J. Comput. Chem.* **2011**, *32*, 1456–1465.
[55] A. Fabrizio, C. Corminboeuf, *J. Phys. Chem. Lett.* **2018**, *9*, 464–470.
[56] F. Zinna, L. Di Bari, in *Lanthanide-Based Multifunctional Materials* (Eds.: P. Martin-Ramos, M. Ramos-Silva), Elsevier, **2018**, pp. 171–194.
[57] H. Kubo, T. Hirose, T. Nakashima, T. Kawai, J. Y. Hasegawa, K. Matsuda, *J. Phys. Chem. Lett.* **2021**, *12*, 686–695.
[58] M. Pecul, K. Ruud, *Phys. Chem. Chem. Phys.* **2011**, *13*, 643–650.
[59] H. R. McAlexander, T. D. Crawford, *J. Chem. Phys.* **2015**, *142*, 154101.
[60] K. Dhbaibi, L. Abella, S. Meunier-Della-Gatta, T. Roisnel, N. Vanthuyne, B. Jamoussi, G. Pieters, B. Racine, E. Quesnel, J. Autschbach, J. Crassous, L. Favereau, *Chem. Sci.* **2021**, *12*, 5522–5533.
[61] F. J. Coughlin, M. S. Westrol, K. D. Oyler, N. Byrne, C. Kraml, E. Zysman-Colman, M. S. Lowry, S. Bernhard, *Inorg. Chem.* **2008**, *47*, 2039–2048.
[62] F. Zinna, T. Bruhn, C. A. Guido, J. Ahrens, M. Bröring, L. Di Bari, G. Pescitelli, *Chem. Eur. J.* **2016**, *22*, 16089–16098.
[63] M. Gon, Y. Morisaki, Y. Chujo, *Eur. J. Org. Chem.* **2015**, *2015*, 7756–7762.
[64] G. Gritzner, J. Kůta, *Pure Appl. Chem.* **1984**, *56*, 461–466.
[65] E. Shabtai, M. Rabinovitz, B. König, B. Knieriem, A. De Meijere, *J. Chem. Soc. Perkin Trans. 2* **1996**, 2589–2595.
[66] R. Jund, P. Lemoine, M. Gross, *Angew. Chem. Int. Ed. Engl.* **1982**, *21*, 305–306; *Angew. Chem.* **1982**, *94*, 312–313.
[67] T. Sato, K. Torizuka, *J. Chem. Soc. Perkin Trans. 2* **1978**, 1199–1204.
[68] A. Schank, B. Speiser, A. Stickel, *J. Electroanal. Chem.* **2016**, *779*, 137–145.
[69] B. Eberle, O. Hübner, A. Ziesak, E. Kaifer, H.-J. Himmel, *Chem. Eur. J.* **2015**, *21*, 8578–8590.
[70] M. Isegawa, F. Neese, D. A. Pantazis, *J. Chem. Theory Comput.* **2016**, *12*, 2272–2284.
[71] A. V. Marenich, C. J. Cramer, D. G. Truhlar, *J. Phys. Chem. B* **2009**, *113*, 6378–6396.
[72] S. Amthor, C. Lambert, *J. Phys. Chem. A* **2006**, *110*, 1177–1189.
[73] J. L. Zafra, A. Molina Ontoria, P. Mayorga Burrezo, M. Peña-Alvarez, M. Samoc, J. Szeremeta, F. J. Ramírez, M. D. Lovander, C. J. Droske, T. M. Pappenfus, L. Echegoyen, J. T. López Navarrete, N. Martín, J. Casado, *J. Am. Chem. Soc.* **2017**, *139*, 3095–3105.
[74] P. Mücke, R. F. Winter, K. Kowalski, *J. Organomet. Chem.* **2013**, *735*, 10–14.
[75] J. Pommerehne, H. Vestweber, W. Guss, R. F. Mahrt, H. Bässler, M. Porsch, J. Daub, *Adv. Mater.* **1995**, *7*, 551–554.
[76] C. M. Cardona, W. Li, A. E. Kaifer, D. Stockdale, G. C. Bazan, *Adv. Mater.* **2011**, *23*, 2367–2371.
[77] R. Holze, *Organometallics* **2014**, *33*, 5033–5042.

Manuscript received: November 19, 2021
Accepted manuscript online: December 17, 2021
Version of record online: January 20, 2022

© 2021 The Authors. Chemistry - A European Journal published by Wiley-VCH GmbH